

# Stereodynamical control of cold collisions between two aligned D<sub>2</sub> molecules

Pablo G. Jambrina

*Departamento de Química Física. Universidad de Salamanca, Salamanca 37008, Spain\**

James F. E. Croft

*The Dood-Walls Centre for Photonic and Quantum Technologies, Dunedin, New Zealand and  
Department of Physics, University of Otago, Dunedin, New Zealand†*

Junxiang Zuo and Hua Guo

*Department of Chemistry and Chemical Biology,  
University of New Mexico, Albuquerque, New Mexico 87131, USA‡*

Naduvath Balakrishnan

*Department of Chemistry and Biochemistry, University of Nevada, Las Vegas, Nevada 89154, USA§*

F. Javier Aoiz

*Departamento de Química Física. Universidad Complutense. Madrid 28040, Spain¶*

(Dated: July 21, 2022)

Resonant scattering of optically state-prepared and aligned molecules in the cold regime allows the most detailed interrogation and control of bimolecular collisions. This technique has recently been applied to collisions of two aligned ortho-D<sub>2</sub> molecules prepared in the  $j = 2$  rotational level of the  $v = 2$  vibrational manifold using the Stark-induced adiabatic Raman passage technique. Here, we develop the theoretical formalism for collisions of two aligned molecules and apply our approach to state-prepared  $D_2(v = 2, j = 2) + D_2(v = 2, j = 2) \rightarrow D_2(v = 2, j = 2) + D_2(v = 2, j = 0)$  collisions. Quantum scattering calculations were performed in full-dimensionality on an accurate H<sub>2</sub>-H<sub>2</sub> interaction potential. Key features of the experimental angular distributions are reproduced and attributed primarily to a partial wave resonance with orbital angular momentum  $\ell = 4$ .

## INTRODUCTION

In molecular encounters collision outcomes are influenced by factors such as the collision energy ( $E_{\text{coll}}$ ) and directional properties (orientation and alignment). While measurements of the energy (actually the kinetic temperature,  $T$ ) dependence of the collision rates are rather routine, experiments that measure the dependence of the outcome of a molecular collision on the initial alignments (stereodynamics) of the reactants are scarce (see for example Refs. 1–19).

Optical state-preparation using the Stark-induced adiabatic Raman passage (SARP) method combined with co-expansion of the colliding species has become a versatile tool to explore stereodynamics of atom-molecule and molecule-molecule collisions [11–13, 18–21]. When applied to light molecules such as HD and D<sub>2</sub>, relative collision energies near  $\sim 1$  K can be achieved, as demonstrated for HD+H<sub>2</sub>/D<sub>2</sub> [11, 12], HD+He [19] and D<sub>2</sub>+He [13, 18] mixtures. In this regime, isolated resonances control the collision outcome, and their strength sometimes depends on the relative alignment between the two partners [22–30], so the SARP method provides a powerful technique to study and control stereodynamics of bimolecular collisions. However, most of these studies involve atom + molecule collisions, and those that deal with bimolecular collisions could only control the

direction of the internuclear axis of one of the colliding partners [11, 12].

Very recently, Zhou *et al.*[31] reported results of the inelastic collisions between two aligned ortho-D<sub>2</sub>( $v=2, j=2$ ) molecules, showing how the angular distribution of the scattered products depends sensitively on the direction of D<sub>2</sub> internuclear axis with regard to the scattering frame defined by  $\mathbf{k}$  and  $\mathbf{k}'$ , the reactant-approach and product-recoil directions. Further, while not directly observed, key features of the angular distribution are attributed to a resonance caused by the orbital angular momentum  $\ell = 2$  near 1 K in the incoming channel whose properties are predicted to be strongly influenced by the initial alignment of the two molecules.

Previous theoretical treatments of the stereodynamics of bimolecular collisions considered only the polarization of one of the collision partners [22–24, 29, 32, 33]. Here, we present the theoretical formalism for the angular distribution of scattered products when both reactants are polarized. Using full-dimensional *ab-initio* quantum scattering calculations on an accurate potential energy surface (PES) [34], we reproduce the experimental angular distributions reported by Zhou *et al.*[31]. Agreement with experiments is only obtained when collisions involving two polarized molecules (both in  $v = 2$ ) as well as one polarized (in  $v = 2$ ) and one unpolarized molecule (in  $v = 0$ , also present in the beam) are considered. Our

results reveal that there is an  $\ell=4$  partial wave resonance whose contribution to the experimental angular distribution is dominant in the 1.5–3.5 K collision energy range.

## METHODS

Let us consider collisions involving two molecules A and B, each of them in a pure rotational state  $j_A$  and  $j_B$  and that we can control the spacial distribution of the internuclear axis of one of them (for example, A). In that case, the state-to-state differential cross section (DCS) can be calculated as [32]

$$d\sigma(\theta|\beta, \alpha) = \sum_{k=0}^{2j} \sum_{q=-k}^k (2k+1) \left[ U_q^{(k)}(\theta) \right]^* a_q^{(k)}, \quad (1)$$

where  $a_q^{(k)}$  are the extrinsic polarization parameters that describe the anisotropic preparation of the reactant in the  $\mathbf{k}-\mathbf{k}'$  scattering frame. If A is prepared in a pure  $|j_A m = 0\rangle$  state, where  $m$  is the magnetic quantum number determined with regard to a laboratory-fixed quantization axis (the polarization vector of the Stokes and pump laser in the SARP experiment), the polarization parameters are given by

$$a_q^{(k)} = C_{kq}(\beta, \alpha) A_0^{(k)} = C_{kq}(\beta, \alpha) \langle j_A 0, k0 | j_A 0 \rangle, \quad (2)$$

where  $A_0^{(k)}$  are the extrinsic polarization parameters in the laboratory frame,  $C_{kq}$  are the modified spherical harmonics, whose arguments  $\beta$  and  $\alpha$  are the polar and azimuthal angles that define the direction of the polarization vector in the scattering frame, and  $\langle \dots | \dots \rangle$  is the Clebsch-Gordan coefficient. For an isotropic internuclear axis distribution, the only non-zero  $a_q^{(k)}$  element is  $a_0^{(0)}$ .

In Eq. 1,  $U_q^{(k)}(\theta)$  are the intrinsic polarization dependent DCSs (PDDCSs) of the  $\{\mathbf{k}-\mathbf{j}_A-\mathbf{k}'\}$  three-vector correlations that describe how the collision outcome depend on the relative geometry of the reactants.  $U_q^{(k)}(\theta)$  can be expressed in terms of the scattering amplitudes in the helicity representation,  $f_{j'_A m'_A j'_B m'_B j_A m_A j_B m_B}(\theta) \equiv F_{m'_A m'_B m_A m_B}(\theta)$ , as:

$$U_q^{(k)}(\theta) = \frac{1}{(2j_A + 1)(2j_B + 1)} \sum_{\substack{m'_A, m'_B \\ m_A, m_B}} F_{m'_A m'_B m_A m_B}(\theta) \times F_{m'_A m'_B (m_A + q) m_B}^*(\theta) \langle j_A m_A, kq | j_A m_A + q \rangle, \quad (3)$$

with

$$F_{m'_A m'_B m_A m_B}(\theta) = \frac{1}{2ik} \sum_J (2J+1) d_{m'_A + m'_B, m_A + m_B}^J(\theta) \times S_{m'_A m'_B m_A m_B}^J(E), \quad (4)$$

where  $d_{m'_A + m'_B, m_A + m_B}^J(\theta)$  is an element of the Wigner reduced rotation matrix, and  $S$  is an element of the Scattering matrix in the helicity representation, with  $m'_A, m'_B,$

$m_A,$  and  $m_B$  being the projections on  $j'_A, j'_B, j_A,$  and  $j_B$  on the initial and final relative velocities, respectively (the primed indices are associated to the products states).

For two polarized reagents under the same polarization vector, the DCS can be expressed as

$$d\sigma(\theta|\beta, \alpha) = \sum_{k_A=0}^{2j_A} \sum_{q_A} \sum_{k_B=0}^{2j_B} \sum_{q_B} (2k_A + 1)(2k_B + 1) \times \left[ U_{q_A, q_B}^{(k_A, k_B)}(\theta) \right]^* a_{q_A}^{(k_A)} a_{q_B}^{(k_B)} \quad (5)$$

where each of the  $a_q^{(k)}$  can be evaluated according to Eq. (2) as a function of the  $\beta$  and  $\alpha$  angles. The intrinsic  $\{\mathbf{k}-\mathbf{j}_A-\mathbf{j}_B-\mathbf{k}'\}$  4-vector PDDCSs,  $U_{q_A, q_B}^{(k_A, k_B)}$ , can be calculated as:

$$U_{q_A, q_B}^{(k_A, k_B)}(\theta) = \frac{1}{(2j_A + 1)(2j_B + 1)} \times \sum_{\substack{m'_A, m'_B \\ m_A, m_B}} F_{m'_A m'_B m_A m_B}(\theta) F_{m'_A m'_B (m_A + q_A) (m_B + q_B)}^*(\theta) \times \langle j_A m_A, k_A q_A | j_A (m_A + q_A) \rangle \langle j_B m_B, k_B q_B | j_B (m_B + q_B) \rangle. \quad (6)$$

If either  $k_A$  or  $k_B$  is zero, we recover the three-vector PDDCS  $U_q^{(k)}(\theta)$ . If  $k_A = k_B = 0$  we recover the  $U_0^{(0)}(\theta)$ , the isotropic DCS.

The DCS in the SARP experiments that we aim to reproduce involves integration over the azimuthal angle ( $\alpha$ ). This allows us to simplify the equation (5) to:

$$d\sigma(\theta|\beta) = 2\pi \sum_{k_A, k_B} (2k_A + 1)(2k_B + 1) U_{0,0}^{(k_A, k_B)}(\theta) \times a_0^{(k_A)} a_0^{(k_B)}. \quad (7)$$

The coupled-channel quantum calculations to evaluate the scattering matrices are carried out in full-dimensionality using a modified version of the TwoBC code [35] and the recently reported full-dimensional PES for the H<sub>2</sub>-H<sub>2</sub> system [34]. This PES was developed by fitting energy points from multi-reference configuration interaction calculations using a permutationally invariant neural network method [36] with the proper electrostatic and long-range dispersion terms. Details of the scattering calculations are given in our prior works [22, 23, 37]. For pure rotational quenching of D<sub>2</sub> ( $v = 2, j = 2$ ), results are insensitive to the inclusion of additional rotational or vibrational levels beyond  $v=2$  and  $j=4$  in the basis set.

## RESULTS

In their experiments, Zhou *et al.* [31] used a collimated D<sub>2</sub> beam with a rotational temperature of  $\approx 130$  K (see SI). Using SARP, nearly all  $|v = 0, j = 0\rangle \equiv |0 0\rangle$ , molecules are transferred to a  $|2 2\rangle$  state. As a result of the pumping process, the D<sub>2</sub> internuclear axes in  $|2 2\rangle$

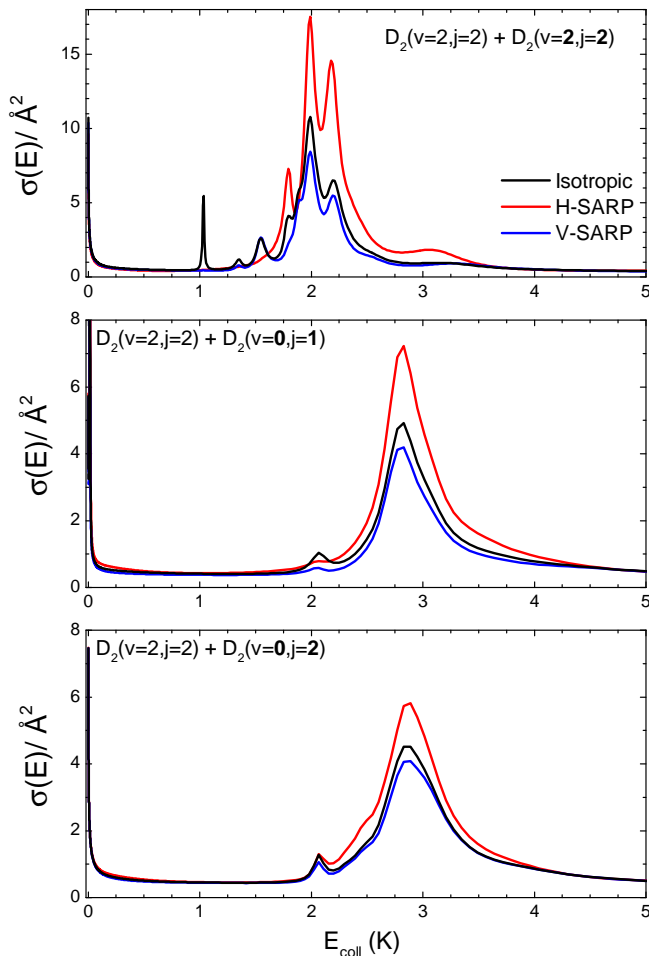


FIG. 1. Excitation functions for  $D_2(v'=2, j'=0)$  production from  $(v=2, j=2) + (v=2, j=2)$  collisions (top panel),  $(v=2, j=2) + (v=0, j=1)$  (middle panel), and  $(v=2, j=2) + (v=0, j=2)$  (bottom panel). Results for isotropic preparation is shown in black, while those for H-SARP ( $\beta=0^\circ$ ), and V-SARP ( $\beta=90^\circ$ ) are shown in red and blue, respectively.

state are aligned in a chosen direction with respect to the molecular beam axis. Here, we will consider three possible scenarios: isotropic (no alignment) internuclear axis distribution, internuclear axis aligned parallel to the molecular beam axis ( $\beta = 0^\circ$  or H-SARP), and internuclear axis of  $D_2$   $|2\ 2\rangle$  aligned perpendicular to the molecular beam axis ( $\beta = 90^\circ$  or V-SARP). After state preparation,  $D_2$  molecules in  $|2\ 2\rangle$  experience collisions with other  $D_2$  molecules in the beam giving rise to a pure rotational de-excitation to the  $|2\ 0\rangle$  state whose angular distribution is selectively detected.

Since all the  $D_2$  molecules travel along the molecular beam spanning a relatively narrow velocity distribution, the relative velocity distribution corresponds to  $E_{\text{coll}} < 5$  K.  $D_2$  in a  $|2\ 0\rangle$  state can be produced from inelastic collisions between either two polarized  $|2\ 2\rangle$  molecules or between one polarized  $|2\ 2\rangle$  and one unpolarized  $|0\ 1\rangle$  or  $|0\ 2\rangle$  partner. The excitation function (cross section as a

function of  $E_{\text{coll}}$ ),  $\sigma(E)$ , for each of these processes are shown in Figure 1. For collisions between  $|2\ 2\rangle$  and  $|0\ 1\rangle$  or  $|0\ 2\rangle$ ,  $\sigma(E)$  is characterized by a broad resonance peak at  $E_{\text{coll}} \sim 2.8$  K and a smaller peak around 2 K, both associated with  $\ell=4$  (see Figure S1). Around the resonance,  $\sigma(E)$  is larger for a H-SARP preparation and slightly smaller for a V-SARP preparation compared to the isotropic case. Away from the resonance,  $\sigma(E)$  is similar for the three preparations of the  $|2\ 2\rangle$  state. In contrast,  $\sigma(E)$  for collisions between two  $|2\ 2\rangle$  molecules displays a complex resonance structure centered around 2 K, which are also enhanced by H-SARP preparation. There is also a sharp resonance at  $E_{\text{coll}} \sim 1$  K, that disappears for both H-SARP and V-SARP polarizations. All these resonances are associated mainly to  $\ell=4$  (see Figure S1) and different values of the total angular momentum  $J$ . Collisions between two  $|2\ 2\rangle$  molecules that lead to two  $|2\ 0\rangle$  products have a significantly smaller cross sections, and hence are not considered here. Irrespective of the  $\sigma(E)$  shape, although the absolute values for collisions between two  $|2\ 2\rangle$  molecules are larger, all the three types of encounters have to be considered to account for the simulation of the experimental angular distributions.

Figure 2 depicts the energy dependent rate coefficients multiplied by the experimental  $E_{\text{coll}}$  distribution, such that its integral over  $E_{\text{coll}}$  is the rate coefficient. The higher flux for the H-SARP preparation is consistent with its larger cross section compared to the V-SARP preparation. The different contributions from the  $v=2$  and  $v=0$  quenchers are also highlighted. At  $E_{\text{coll}}$  within 1.5–2.5 K, the flux mostly originates from the resonance features due to  $(v=2) + (v=2)$  collisions, whereas at higher energies the broad resonance due to  $(v=2) + (v=0)$  collisions prevails. Overall, the energy distributions reflect the interplay between resonance features associated with  $(v=2) + (v=2)$  and  $(v=2) + (v=0)$  collision partners, all of them associated to  $\ell=4$  (instead of  $\ell=2$  as discussed in Ref. [31]), and also show contributions from lower energies, associated to  $\ell=0$  and 1 (see Figure S2).

Figure 3 shows the computed angular distributions (differential rate coefficients) convoluted over the experimental velocity distributions for the three collision pairs considered here and the H-SARP and V-SARP preparations. Since in the experiments it is not possible to distinguish between products scattered at  $\theta$  or  $\pi-\theta$  (where  $\theta$  is the scattering angle, that between  $\mathbf{k}$  and  $\mathbf{k}'$ ), the angular distributions are symmetrized as in the experiments [31]. For H-SARP preparations between two polarized  $|2\ 2\rangle$  molecules we observe prominent peaks at  $15^\circ$  and  $165^\circ$ . These peaks are also present for  $|2\ 2\rangle + |0\ 1\rangle$  collisions, although in that case, they are not that dominant, and peaks at  $60^\circ$ ,  $90^\circ$ , and  $120^\circ$  also exist. For  $|2\ 2\rangle + |0\ 2\rangle$  collisions the shape is similar but the magnitude is smaller for the most forward and backward peaks. The sharp peaks observed for  $|2\ 2\rangle + |2\ 2\rangle$  are a consequence

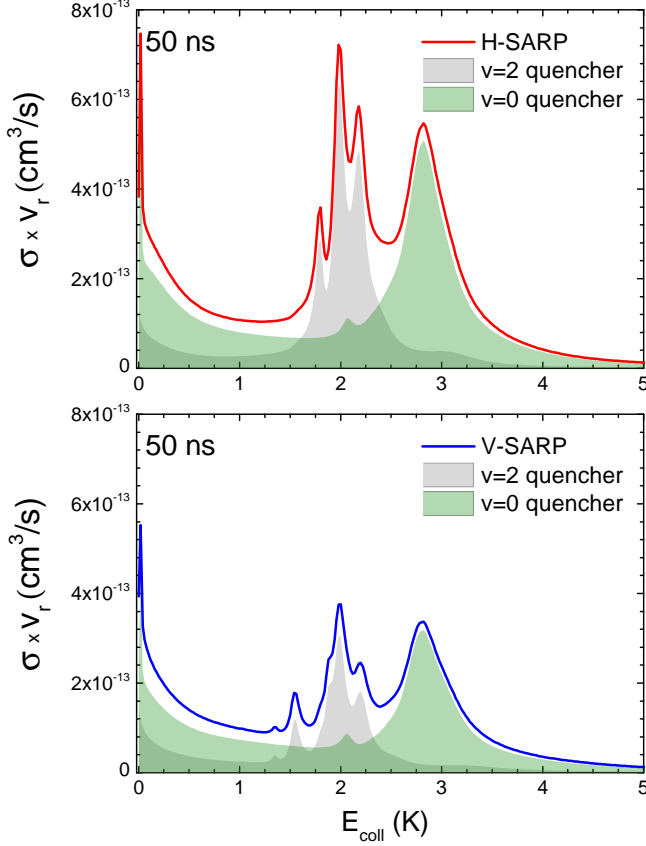


FIG. 2. Energy dependent integral rate coefficients multiplied by the experimental collision energy distribution for a 50 ns SARP-REMPI delay time for the two experimental preparations: H-SARP ( $\beta=0^\circ$ ) (top panel) and V-SARP ( $\beta=90^\circ$ ) (bottom panel). The contribution of collisions between two  $D_2(v=2)$  molecules is highlighted in shaded in grey while that from collisions between one  $D_2(v=2)$  and one  $D_2(v=0)$  molecule is shown in shaded dark green.

of the simultaneous polarization of both  $D_2$  molecules. If, incorrectly, the simulation is carried out just considering polarization of one of the two partners, the shape of the angular distribution is similar to that obtained for  $|2\ 2\rangle + |0\ 1\rangle$  (see Figure S3). For a V-SARP preparation, we obtain a salient  $90^\circ$  peak for  $|2\ 2\rangle + |2\ 2\rangle$  collisions that is somewhat suppressed for  $|2\ 2\rangle + |0\ 1\rangle$  encounters. The angular distribution for  $|2\ 2\rangle + |0\ 2\rangle$  collisions shows a small dip at  $90^\circ$  with small shoulders at each side at  $70^\circ$  and  $110^\circ$ .

Taking into account the populations of the different rovibrational states in the beam, it is possible to combine the angular distributions depicted in Figure 3 and compare with the experimental angular distributions. Such a comparison is presented in Figure 4. Note that experiments do not provide absolute values of DCS, so comparison is made on a relative scale. The agreement between experiment and calculations is good for both H-SARP and V-SARP. For H-SARP our calculations predict that

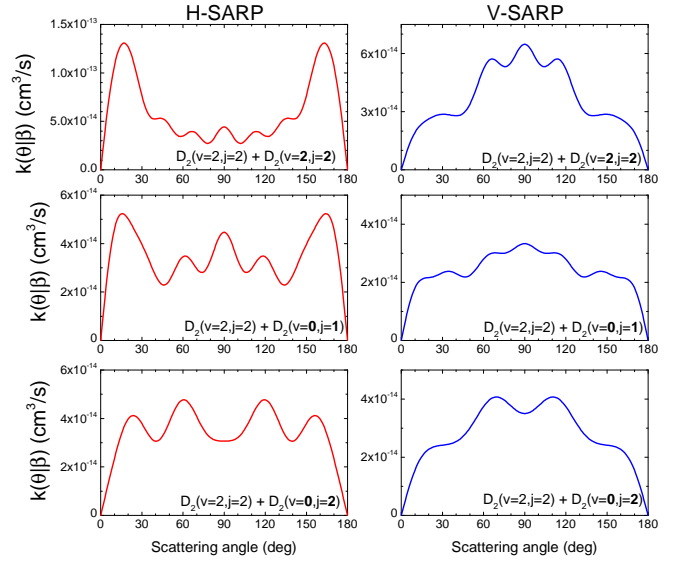


FIG. 3. Velocity-averaged differential rate coefficients for  $D_2(v'=2, j'=0)$  production from  $(v=2, j=2) + (v=2, j=2)$  collisions (top panel),  $(v=2, j=2) + (v=0, j=1)$  (middle panel), and  $(v=2, j=2) + (v=0, j=2)$  (bottom panel). Results for a H-SARP (V-SARP) preparation are shown in the left (right) panel. Differential rate coefficients were symmetrized as discussed in the text.

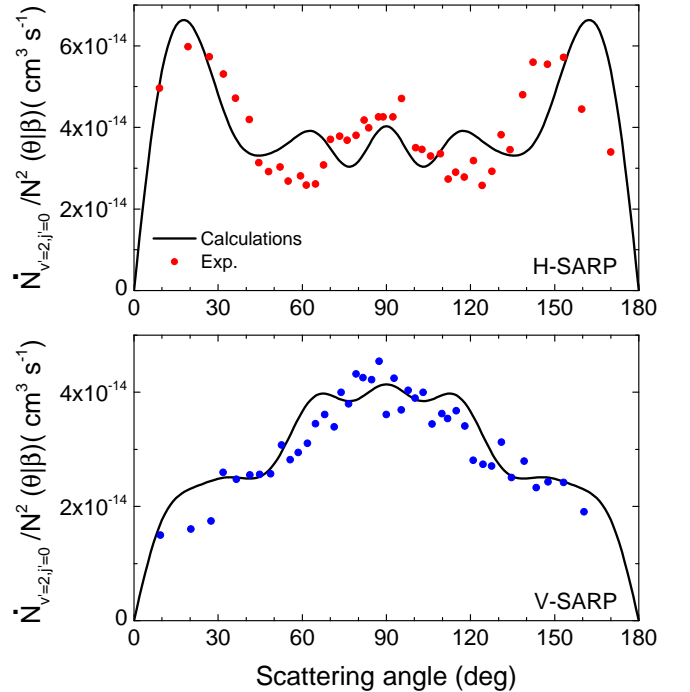


FIG. 4. Initial molecular state and velocity-averaged differential rate coefficients for  $D_2(v'=2, j'=0)$  production normalized by the square of the total density of  $D_2$  (see SI for further details). Results of our calculations are shown in solid curves while experimental results of Zhou *et al.*[31] are shown in dots. Calculations using a H-SARP (V-SARP) preparation are shown in the top (bottom) panels. Differential rate coefficients were symmetrized as in the experimental work.

forward and backward experimental peaks are caused by  $|2\ 2\rangle + |2\ 2\rangle$  collisions while collisions between  $|2\ 2\rangle + |0\ 1\rangle$  and  $|0\ 2\rangle$  contribute to sideways scattering and, in particular, to the smaller sideways peaks. Regarding V-SARP, the experimental signatures primarily arise from the  $|2\ 2\rangle + |2\ 2\rangle$  collisions modulated by small contributions from the other two collision pairs.

Altogether, our results provide a complete *ab initio* simulation of the experiments of Zhou *et al.* [31] on stereodynamics of bimolecular collisions between two aligned  $D_2$  molecules. This is enabled by developing the theory for stereodynamics of aligned-aligned bimolecular collisions and by considering different collision processes that occur in the molecular beam. Results presented here based on full-dimensional coupled-channel scattering calculations reveal that the angular distribution observed in the experiments of Zhou *et al.* [31] is due to resonance features that arise from different collision partners in the beam with distinct angular distributions. The formalism presented here is general, and will provide the foundation for describing four-vector correlation in reactive or inelastic aligned molecular collisions in future experiments involving SARP or related techniques.

#### ACKNOWLEDGEMENT

This work was supported in part by NSF grant No. PHY-2110227 (N.B.) and ARO MURI grant No. W911NF-19-1-0283 (N.B., H.G.). P.G.J. gratefully acknowledges grant PID2020-113147GA-I00 funded by MCIN/AEI/10.13039/, and F.J.A. acknowledges funding by the Spanish Ministry of Science and Innovation (Grants No. PGC2018-096444-B-I00 and PID2021-122839NB-I00). J.F.E.C gratefully acknowledges support from the Dodd-Walls Centre for Photonic and Quantum Technologies.

---

\* pjambrina@usal.es

† j.croft@otago.ac.nz

‡ hguo@unm.edu

§ naduvala@unlv.nevada.edu

¶ aoiz@quim.ucm.es

- [1] F. Wang, J. S. Lin, and K. Liu, *Science* **331**, 900 (2011).
- [2] F. Wang, K. Liu, and T. P. Rakitzis, *Nat. Chem.* **4**, 636 (2012).
- [3] F. Wang and K. Liu, *J. Chem. Phys.* **145**, 144305 (2016).
- [4] F. Wang and K. Liu, *J. Chem. Phys.* **145**, 144306 (2016).
- [5] M. Brouard, H. Chadwick, S. Gordon, B. Hornung, B. Nichols, F. J. Aoiz, and S. Stolte, *J. Phys. Chem. A* **119**, 12404 (2015).
- [6] H. Chadwick, B. Nichols, S. D. S. Gordon, B. Hornung, E. Squires, M. Brouard, J. Klos, M. H. Alexander, F. J. Aoiz, and S. Stolte, *J. Phys. Chem. Lett.* **5**, 3296 (2014).
- [7] M. Brouard, H. Chadwick, C. J. Eyles, B. Hornung, B. Nichols, F. J. Aoiz, P. G. Jambrina, and S. Stolte, *J. Chem. Phys.* **138**, 104310 (2013).
- [8] S. N. Vogels, T. Karman, J. Klos, M. Besemer, J. Onvlee, J. O. van der Avoird, G. C. Groenenboom, and S. Y. T. van de Meerakker, *Nat. Chem.* **10**, 435 (2018).
- [9] J. Onvlee, S. D. S. Gordon, S. N. Vogels, T. Auth, T. Karman, B. Nichols, A. van der Avoird, G. C. Groenenboom, M. Brouard, and S. Y. T. van de Meerakker, *Nat. Chem.* **9**, 226 (2017).
- [10] T. R. Sharples, J. G. Leng, T. F. M. Luxford, K. G. McKendrick, P. G. Jambrina, F. J. Aoiz, D. W. Chandler, and M. L. Costen, *Nat. Chem.* **10**, 1148 (2018).
- [11] W. E. Perreault, N. Mukherjee, and R. N. Zare, *Science* **358**, 356 (2017).
- [12] W. E. Perreault, N. Mukherjee, and R. N. Zare, *Nat. Chem.* **10**, 561 (2018).
- [13] H. Zhou, W. E. Perreault, N. Mukherjee, and R. N. Zare, *J. Chem. Phys.* **154**, 104309 (2021).
- [14] C. G. Heid, V. Walpole, M. Brouard, P. G. Jambrina, and F. J. Aoiz, *Nat. Chem.* **11**, 662 (2019).
- [15] C. G. Heid, I. P. Bentham, V. Walpole, P. G. Jambrina, F. J. Aoiz, and M. Brouard, *J. Phys. Chem. Lett.* **12**, 310 (2021).
- [16] C. G. Heid, I. P. Bentham, V. Walpole, R. Gheorge, P. G. Jambrina, F. J. Aoiz, and M. Brouard, *Phys. Chem. Chem. Phys.* **22**, 22289 (2020).
- [17] V. Walpole, C. G. Heid, P. G. Jambrina, F. J. Aoiz, and M. Brouard, *J. Phys. Chem. A* **123**, 8787 (2019).
- [18] H. Zhou, W. E. Perreault, N. Mukherjee, and R. N. Zare, *Science* **374**, 960 (2021).
- [19] W. E. Perreault, N. Mukherjee, and R. N. Zare, *J. Chem. Phys.* **150**, 174301 (2019).
- [20] C. Amarasinghe and A. G. Suits, *J. Phys. Chem. Lett.* **8**, 5153 (2017).
- [21] C. Amarasinghe, C. A. Perera, and A. G. Suits, *J. Chem. Phys.* **152**, 184201 (2020).
- [22] J. F. E. Croft, N. Balakrishnan, M. Huang, and H. Guo, *Phys. Rev. Lett.* **121**, 113401 (2018).
- [23] J. F. E. Croft and N. Balakrishnan, *J. Chem. Phys.* **150**, 164302 (2019).
- [24] P. G. Jambrina, J. F. E. Croft, H. Guo, M. Brouard, N. Balakrishnan, and F. J. Aoiz, *Phys. Rev. Lett.* **123**, 043401 (2019).
- [25] M. Morita and N. Balakrishnan, *J. Chem. Phys.* **153**, 091101 (2020).
- [26] M. Morita and N. Balakrishnan, *J. Chem. Phys.* **153**, 184307 (2020).
- [27] M. Morita, Q. Yao, C. Xie, H. Guo, and N. Balakrishnan, *Phys. Rev. Research* **2**, 032018(R) (2020).
- [28] P. G. Jambrina, L. González-Sánchez, M. Lara, M. Menéndez, and F. J. Aoiz, *Phys. Chem. Chem. Phys.* **22**, 24943 (2020).
- [29] P. G. Jambrina, J. F. E. Croft, N. Balakrishnan, and F. J. Aoiz, *Phys. Chem. Chem. Phys.* **23**, 19364 (2021).
- [30] P. G. Jambrina, M. Morita, J. F. E. Croft, F. J. Aoiz, and N. Balakrishnan, *J. Phys. Chem. Lett.* **13**, 4064 (2022).
- [31] H. Zhou, W. E. Perreault, N. Mukherjee, and R. N. Zare, *Nat. Chem.* **14**, (2022).
- [32] J. Aldegunde, M. P. de Miranda, J. M. Haigh, B. K. Kendrick, V. Saez-Rabanos, and F. J. Aoiz, *J. Phys. Chem. A* **109**, 6200 (2005).
- [33] D. Yang, D. Xie, and H. Guo, *J. Phys. Chem. Lett.* **13**, 1777 (2022).

- [34] J. Zuo, J. F. E. Croft, Q. Yao, N. Balakrishnan, and H. Guo, *J. Chem. Theory Comput.* **17**, 6747 (2021).
- [35] R. Krens, TwoBC – quantum scattering program, University of British Columbia, Vancouver, Canada, 2006.
- [36] B. Jiang, J. Li, and H. Guo, *Int. Rev. Phys. Chem.* **35**, 479 (2016).
- [37] G. Quéméner and N. Balakrishnan, *J. Chem. Phys.* **130**, 114303 (2009).
- [38] W. M. Huo and S. Green, *J. Chem. Phys.* **104**, 7572 (1996).
- [39] D. L. Johnson, R. S. Grace, and J. G. Skofronick, *J. Chem. Phys.* **71**, 4554 (1979).

SUPPLEMENTARY INFORMATION

CALCULATION OF INITIAL MOLECULAR STATE AND VELOCITY-AVERAGED DIFFERENTIAL RATE COEFFICIENTS

The experiments by Zhou *et al.* [31] made use of a collimated D<sub>2</sub> beam in which 38% of the molecules are in ( $v=0, j=0$ ), 36% in ( $v=0, j=1$ ), and 24% in a ( $v=0, j=2$ ) state. After the SARP preparation, nearly all molecules in ( $v=0, j=0$ ) are pumped to ( $v=2, j=2$ ). Experimentally, it was possible to select the distribution of the D<sub>2</sub>( $v=2, j=2$ ) internuclear axis in the scattering frame by changing the direction of polarization of the laser pulses, defined by the angles  $\beta$  and  $\alpha$  with respect to the scattering frame. Molecules in D<sub>2</sub>( $v'=2, j'=0$ ) resulting from rotationally inelastic collisions between two D<sub>2</sub> molecules were probed by (2+1) REMPI, and from the velocity distribution of the scattered products, the angular distribution could be extracted. Although the speed of the D<sub>2</sub> molecules is about 2 km/s, relative collision energies,  $E_{\text{coll}}$ , are below 5 K, so D<sub>2</sub>( $v'=2, j'=0$ ) can only be produced by quenching of D<sub>2</sub>( $v=2, j=2$ ). Hence,  $\dot{N}_{v'=2, j'=0}(\theta|\beta)$ , the flux of the scattered D<sub>2</sub>( $v'=2, j'=0$ ) can be calculated as:

$$\dot{N}(v' = 2, j' = 0, \theta|\beta) \equiv \frac{dN(v' = 2, j' = 0, \theta|\beta)}{dt} = \frac{1}{2} k_{22,22}(\theta|\beta) N_{22} N_{22} + k_{22,01}(\theta|\beta) N_{22} N_{01} + k_{22,02}(\theta|\beta) N_{22} N_{02} \quad (\text{S.1})$$

where  $k_{v_A j_A, v_B j_B}(\theta|\beta)$  are the differential rate coefficients for collisions between D<sub>2</sub> molecules in ( $v_A, j_A$ ) and ( $v_B, j_B$ ) states calculated as

$$k(\theta|\beta) = \int d\sigma(\theta|\beta) \sin \theta \sqrt{\frac{2E_{\text{coll}}}{\mu}} f(E_{\text{coll}}) dE_{\text{coll}} \quad (\text{S.2})$$

in which  $\mu$  is the reduced mass of D<sub>2</sub>+D<sub>2</sub> and  $f(E_{\text{coll}})$  the experimental energy distribution. In Eq. (S.1),  $N_{v,j}$  is the molecular density for the ( $v, j$ ) state. The 1/2 factor in  $k_{22,22}$  is not to count twice collisions of two D<sub>2</sub> molecules in the same |2 2> state.

Since the total density of D<sub>2</sub> in the experiment is unknown, the results shown in Figure 4 are calculated by replacing absolute densities,  $N_{v,j}$  by their relative values  $n_{v,j} = N_{v,j}/N$ , where  $N$  is the total D<sub>2</sub> density in the molecular beam. Hence the products of the relative densities are  $n_{22}n_{22}/2 = 0.2405$ ,  $n_{22}n_{01} = 0.4556$ , and  $n_{22}n_{02} = 0.3037$ .

In Eq. (S.1) we only consider collisions in which only one D<sub>2</sub>( $v=2, j=2$ ) is quenched to D<sub>2</sub>( $v'=2, j'=0$ ) while its collision partner is unperturbed. Double relaxation collisions, albeit possible, are associated with much lower cross sections and their contribution to the experiment is negligible.

Collisions between ( $v=2, j=2$ ) and ( $v=0, j=1$ ) involve one *o*-D<sub>2</sub> and one *p*-D<sub>2</sub> molecules, which are distinguishable. However, collisions between ( $v=2, j=2$ ) and ( $v=0, 2, j=2$ ) involve two indistinguishable *o*-D<sub>2</sub> molecules. To carry out calculations for two indistinguishable molecules, the wave function was symmetrized with respect to the exchange-permutation symmetry of the molecules,[37] and the statistically weighted sum of the exchange-permutation symmetrized cross sections is given by [38]

$$\sigma_{j'_A j'_B, j_A j_B} = w^+ \sigma_{j'_A j'_B, j_A j_B}^+ + w^- \sigma_{j'_A j'_B, j_A j_B}^- \quad (\text{S.3})$$

where  $w^\pm$  are the statistical weights of nuclear spin states associated with even or odd exchange symmetries of the two identical D<sub>2</sub> nuclei. In the particular case of collisions between two *o*-D<sub>2</sub> molecules [39],

$$w^+ = \frac{21}{36}, \quad w^- = \frac{15}{36}. \quad (\text{S.4})$$

An equation similar to (S.3) holds for the calculation of any other observable when indistinguishable particles are involved, such as  $d\sigma(\theta|\beta, \alpha)$ :

$$d\sigma(\theta|\beta, \alpha) = w^+ d\sigma^+(\theta|\beta, \alpha) + w^- d\sigma^-(\theta|\beta, \alpha) \quad (\text{S.5})$$

where the scattering amplitudes are given by

$$F_{m'_A m'_B, m_A m_B}^\pm(\theta) = \frac{1}{2ik} \sum_J (2J+1) d_{m'_A + m'_B, m_A + m_B}^J(\theta) S_{m'_A m'_B, m_A m_B}^{J, \pm}(E). \quad (\text{S.6})$$

In the particular case of  $(v=2, j=2) + (v=0, j=2)$  collisions,  $S_{m'_A m'_B m_A m_B}^{J,+}(E) \sim S_{m'_A m'_B m_A m_B}^{J,-}(E)$ . As discussed by Huo and Green [38] this implies that the two collision partners are virtually distinguishable (there is no interference between the direct and exchange mechanisms, the latter being negligible). On the contrary, for the  $(v=2, j=2) + (v=2, j=2)$  collisions  $S^{J,+}$  and  $S^{J,-}$  are very different, which is indicative of a strong interference between direct and exchange mechanisms.



## CONTRIBUTION OF $\ell$ PARTIAL WAVES TO THE EXCITATION FUNCTIONS

In this section we present the decomposition of the integral cross sections into the various contributions from the orbital angular momentum  $\ell$ -partial waves.

Figure S1 displays the contributions from  $\ell = 2$  and  $\ell = 4$  to the isotropic (unaligned  $D_2$  molecules) integral cross sections (excitation functions) for  $D_2(v = 2, j = 2) + D_2(v = 2, j = 2) \rightarrow D_2(v = 2, j = 0) + D_2(v = 2, j = 2)$  (top panel),  $D_2(v = 2, j = 2) + D_2(v = 0, j = 1) \rightarrow D_2(v = 2, j = 0) + D_2(v = 0, j = 1)$  (middle panel), and  $D_2(v = 2, j = 2) + D_2(v = 0, j = 2) \rightarrow D_2(v = 2, j = 0) + D_2(v = 0, j = 2)$  (lower panel). As can be seen, the prevailing contribution in all cases is that from  $\ell = 4$ . Specifically, the resonances for quenching with  $D_2(v = 0, j = 1, 2)$  are exclusively due to the  $\ell = 4$ .

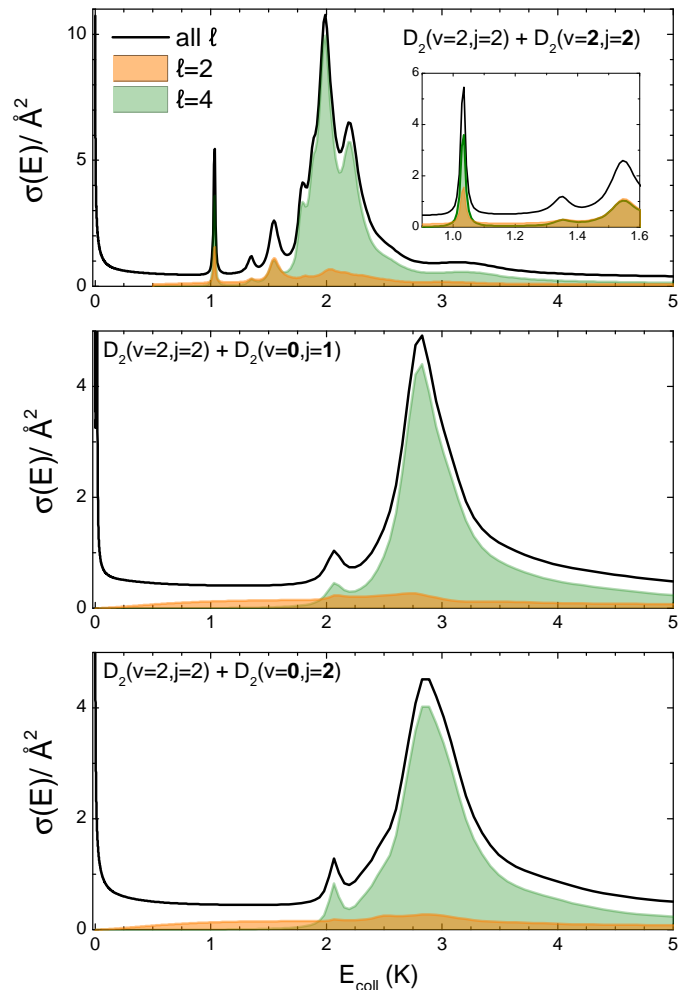


Fig. S1. Isotropic excitation functions for  $D_2(v'=2, j'=0)$  production from  $(v=2, j=2) + (v=2, j=2)$  collisions (top panel),  $(v=2, j=2) + (v=0, j=1)$  (middle panel), and  $(v=2, j=2) + (v=0, j=2)$  (bottom panel). Results for all  $\ell$  are shown by black curves, while those including only  $\ell=2$  and  $\ell=4$  are shaded in orange and green, respectively. As it is apparent from the figure, resonances are caused mainly by  $\ell=4$ , although there is a small contribution from  $\ell=2$ .

Figure S2 shows the energy dependent flux (multiplied by the relative collision energy distribution at 50 ns) in the isotropic case including the contributions from all the possible quenchers. The total flux is broken down into the various  $\ell$  contributions. As can be seen,  $\ell=4$  contributes mostly to the scattering, with  $\ell=0$ , and 1 becoming prominent at  $E_{\text{coll}} < 1$  K.

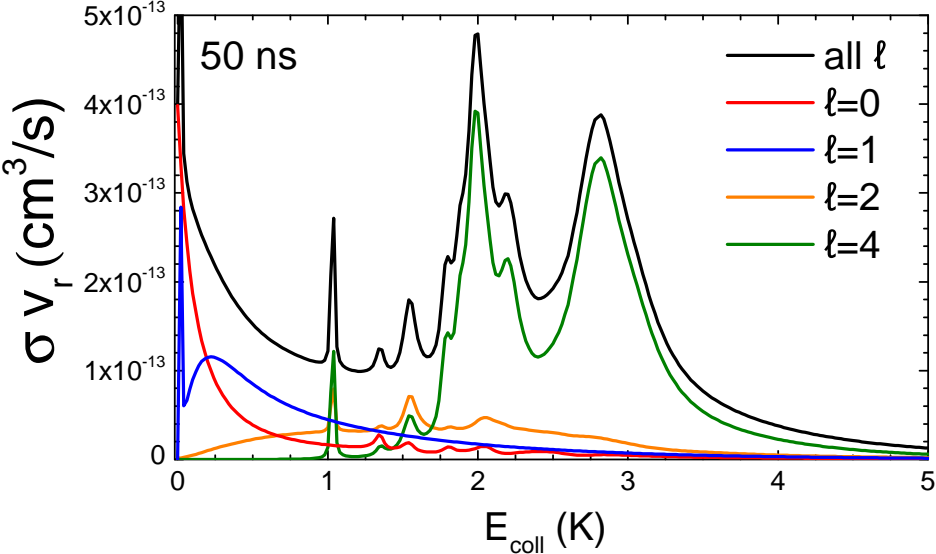


Fig. S2. Energy dependent flux weighted with energy distribution for an isotropic preparation comprising all the possible quenchers. The contributions from different  $\ell$  partial waves are also shown.

### DIFFERENCES BETWEEN THREE- AND FOUR-VECTOR CORRELATIONS

To properly account for the experiments, polarization of both molecules should be considered in the collisions between two indistinguishable  $\text{D}_2$  ( $v=2, j=2$ ) molecules, and 4-vector  $\{\mathbf{k}-\mathbf{j}_A-\mathbf{j}_B-\mathbf{k}'\}$  correlations are needed. To assess the importance of the 4-vector correlations, Figure S3 shows the effect of simulating the velocity-averaged differential rate coefficients using only three-vector PDDCSs (i.e., a scenario in which only one of the two partners is polarized). As can be seen, for V-SARP there is almost no difference, while for H-SARP we observe how the two prominent peaks at  $15^\circ$  and  $165^\circ$  are significantly less intense when 4-vector PDDCSs are not included. Actually, the neglect of 4-vector correlations leads to velocity-averaged differential rate coefficients with a similar shape as those obtained for  $\text{D}_2$  ( $v=2, j=2$ ) +  $\text{D}_2$  ( $v=2, j=1,2$ ) collisions.

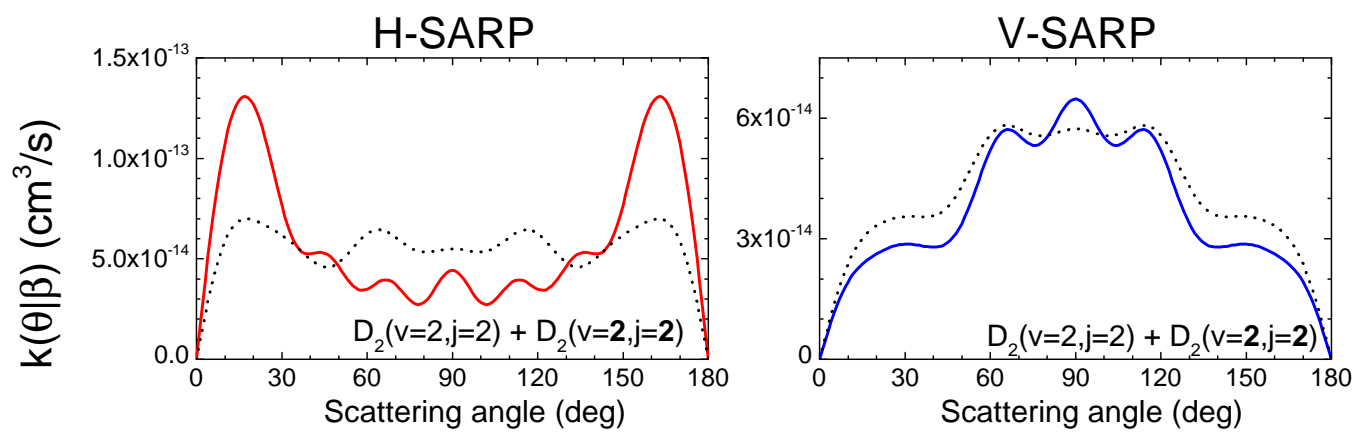


Fig. S3. Velocity-averaged differential rate coefficients for  $D_2(v'=2, j'=0)$  production from  $(v=2, j=2) + (v=2, j=2)$  collisions considering the full (4-vector) correlations (solid lines) and a scenario where only two of the two partners is polarized (dashed line).